Enhanced Magnon Spin Current Using the Bosonic Klein Paradox

J.S. Harms[1,*] H.Y. Yuan,[1,†] and Rembert A. Duine[1,2]

[1]*Institute for Theoretical Physics, Utrecht University, Utrecht 3584CC, Netherlands*

[2]*Department of Applied Physics, Eindhoven University of Technology, P.O. Box 513, Eindhoven 5600 MB, Netherlands*

Efficient manipulation of magnons for information processing is a central topic in spintronics and magnonics. An outstanding challenge for long-distance spin transport with minimal dissipation is to overcome the relaxation of magnons and to amplify the spin current they carry. Here, we propose to amplify magnon currents based on the realization of the bosonic Klein paradox in magnetic nanostructures. This paradox involves the antimagnon, carrying opposite spin and energy, the existence of which is usually precluded by ferromagnetic instabilities, as it is an excitation at negative energy. We show that by appropriately tuning the effective dissipation through spin-orbit torques, both magnons and antimagnons are dynamically stabilized. As a result, we find that the reflection coefficient of incident magnons at an interface between two coupled magnets can become larger than one, thereby amplifying the reflected magnon current. Our findings can lead to magnon amplifier devices for spintronic applications. Furthermore, our findings yield a solid-state platform to study the relativistic behavior of bosonic particles, which is an outstanding challenge with fundamental particles.

I. INTRODUCTION

Spin waves, and their quanta called magnons, are collective excitations that occur in ordered magnets. The emerging field of magnonics utilizes magnons for information processing [1]. As information carriers, magnons have the advantages of low power consumption and efficient parallel data processing, as they do not give rise to Joule heating. Furthermore, they are useful for both classical information processing, which includes logic gates [2,3], transistors [4–7], and diodes [8], and for quantum science and technologies, including single-magnon states, squeezed states, and entanglement with other quantum platforms [9–13]. A hurdle to be overcome in realizing magnon-based technology is the dissipation of magnons, which results from interactions of magnons with their environment, such as conduction electrons, phonons, and impurities. These interactions dissipate the amplitude and coherence of magnon currents and are detrimental for efficient application of magnons in nanoscale spintronic devices. Therefore, a central challenge in magnonics is to counteract the effect of magnon dissipation and to find reliable "control knobs" to sustain the magnon current for long-distance transport. It has been proposed that

magnon Bose-Einstein condensates [14,15], spin superfluids [16,17], the spin Hall effect [18], thermal spin torques [19], topological edge-mode generation [20], and non-Hermitian coupling with cavity photons [21] can be used to enhance magnon currents.

In this paper, we show that the magnon spin current can be significantly amplified at an interface between a magnet that is not driven externally and a magnet into which angular momentum is injected using spin-orbit torque (SOT) [22–26]. By designing the balance of this external driving with intrinsic dissipation, both magnons (positive-energy excitations) and antimagnons (negative-energy excitations) are dynamically stabilized. This results in enhanced reflection of magnons from the interface with the driven-dissipative magnet. The enhanced reflection is accompanied by a transmitted antimagnon current. This suggests a method to amplify magnon spin currents that is relatively straightforward to implement, which may be generalized to both ferromagnetic and antiferromagnetic materials, to different types of driving, and to both metals and insulators. Below, we explicitly illustrate the basic physics for a magnetic heterostructure involving yttrium iron garnet (YIG) and platinum.

Our result can be interpreted as a realization of the bosonic Klein paradox, which refers to the counterintuitive reflection or transmission of relativistic particles from a potential barrier [27–32], and is a natural consequence of quantum field theories. The experimental test of

---

*j.s.harms@uu.nl

†huaiyangyuan@gmail.com

this paradox using fundamental particles is nearly impossible because of the extremely high energy barrier that needs to be overcome [33]. While its solid-state realization for fermionic particles in two-dimensional materials with gapless excitations has recently been reported [34–36], the study of the Klein paradox for bosonic quasiparticles remains an outstanding challenge because the presence of bosonic antiparticles in a solid-state system usually signals instabilities. In our implementation, these instabilities are prevented by the external driving via SOT. Hence, in addition to the application-motivated magnon amplification that is discussed above, our results launch driven magnetic systems as a suitable solid-state platform to experimentally study the field-theoretical physics of bosonic particles.

II. PHYSICAL MODEL

A. Setup and magnonic and antimagnonic excitations

We consider two exchange-coupled ferromagnetic (FM) insulating thin films adjacent to a heavy-metal layer (HM) subject to an in-plane external magnetic field in the z direction, as shown in Fig. 1(a). The magnetization of the right FM aligns antiparallel to the external field. This situation is energetically unstable but dynamically stable due to the presence of an electric current in the HM layer, which exerts a SOT on the magnetization dynamics. This can be understood as follows: the spin current produced by the electric current through the spin Hall effect in the HM will keep injecting angular momentum to the FM layer to counteract the damping of magnetization and to prevent the magnetization to align with the external field, thereby yielding a region with dynamically stable antimagnons. In general, the dynamics of the magnetization, $\mathbf{n}_\nu = \mathbf{M}_\nu/M_s$, are well described by the Landau-Lifschitz-Gilbert (LLG) equation with SOT [26], i.e.,

$$\frac{\partial \mathbf{n}_\nu}{\partial t} = -\gamma \mathbf{n}_\nu \times \mathbf{h}_{\text{eff},\nu} + \alpha \mathbf{n}_\nu \times \frac{\partial \mathbf{n}_\nu}{\partial t} + J_\nu \mathbf{n}_\nu \times \hat{z} \times \mathbf{n}_\nu, \tag{1}$$

where $\nu = L, R$ labels the (L)eft and (R)ight magnets, γ is the gyromagnetic ratio, α is the Gilbert damping, and J_ν characterizes the strength of the SOTs generated by the spin current, which depends on the current flowing in the HM layer, the spin Hall angle of the HM, and the properties of the interface. The LLG equation describes damped precession around the effective magnetic field, $\mathbf{h}_{\text{eff},\nu} = -\delta E_\nu/(M_s \delta \mathbf{n}_\nu)$, where M_s is the saturation magnetization. Here, we consider the magnetic energy functional $E_\nu[\mathbf{n}_\nu]$ in the left and right magnet to be of the form

$$E_\nu = \int dV \left\{ A(\nabla_i \mathbf{n}_\nu)^2 - \mu_0 H_{e,\nu} M_s n_{z,\nu} + \frac{1}{2} K n_{y,\nu}^2 \right\}, \tag{2}$$

where A is the exchange stiffness, $H_{e,\nu}$ is the external magnetic field strength, μ_0 is the vacuum permeability, and
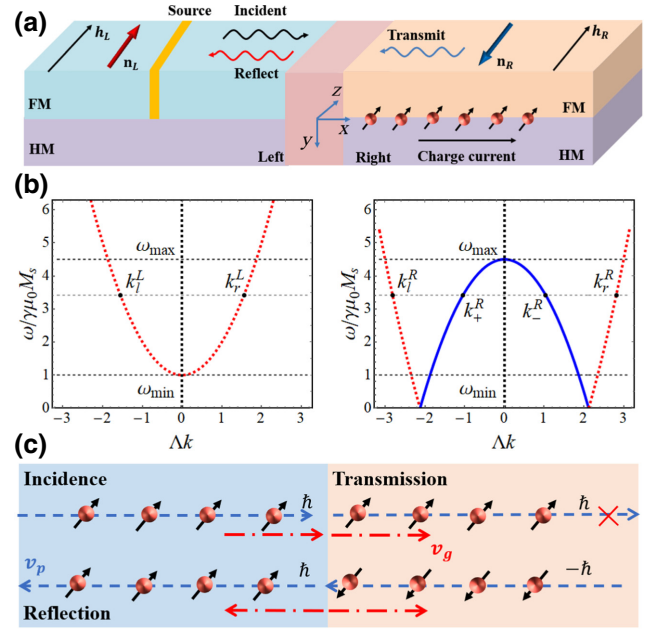

FIG. 1. (a) A schematic of the driven-dissipative magnetic system containing two exchange-coupled magnetic films. (b) The magnon dispersion for the left and right ferromagnets, respectively. The red dotted curves give the positive-energy excitations, while the blue curve corresponds to the negative-energy excitations. In other words, negative-energy excitations exist for the wave numbers $-2.1 \lesssim \Lambda k \lesssim 2.1$ between the zeros of the dispersion in the right magnet. (c) A physical picture of the anomalous magnon reflection. The blue and red arrows represent the directions of the phase and group velocity, respectively.

$K = \mu_0 M_s^2$ is the effective shape anisotropy caused by the dipolar interaction.

Spin waves or magnons are introduced as linear dynamical fluctuations on top of the equilibrium magnetization $\mathbf{n}_{0,\nu}$ with $\mathbf{n}_{0,L} = e_z$ and $\mathbf{n}_{0,R} = -e_z$. By introducing the complex field $\Psi_\nu = (1/\sqrt{2})(\hat{x} \mp i\hat{y}) \cdot \mathbf{n}_\nu$, the linearized LLG equation [37–39] accordingly becomes

$$\frac{i(\mathbb{1} + i\alpha\sigma_z)\partial_t}{\gamma\mu_0 M_s} \begin{pmatrix} \Psi_\nu \\ \Psi_\nu^* \end{pmatrix} = (\mathcal{L}_\pm + iI_\nu \mathbb{1}) \begin{pmatrix} \Psi_\nu \\ \Psi_\nu^* \end{pmatrix}, \tag{3}$$

where

$$\mathcal{L}_\pm = (\Delta \pm h_\nu - \Lambda^2 \nabla^2)\sigma_z + i\Delta\sigma_y. \tag{4}$$

In the above, $\sigma_{y,z}$ are the Pauli matrices, $\Lambda = \sqrt{2A/\mu_0 M_s^2}$ is the exchange length, $h_\nu = H_{e,\nu}/M_s$ is the dimensionless external magnetic field, $\Delta = K/2\mu_0 M_s^2 = 1/2$ is the dimensionless anisotropy constant, and $I_\nu = J_\nu/\gamma\mu_0 M_s$ is the dimensionless SOT. The $\pm$ sign in the definition of Ψ_ν and Eqs. (3) and (4) comes from the linearization around the $\pm e_z$ direction in the left and right ferromagnets, respectively. We introduce spin-wave solutions of the linearized

LLG equation [see Eq. (3)] in the form of the Bogoliubov modes

$$\Psi_\nu(\mathbf{x}, t) = u_\nu(\mathbf{x})e^{-i\lambda t} - v_\nu^*(\mathbf{x})e^{i\lambda^* t}. \qquad (5)$$

Here, the Fourier transforms of $u_\nu(\mathbf{x})$ and $v_\nu(\mathbf{x})$ satisfy, up to first order in α and I_ν, the following dispersion relation:

$$\omega_{\mathbf{k},\nu} \simeq \omega_{\mathbf{k},\nu}^0 - i\left(\alpha\left[\Delta \pm h_\nu - \Lambda^2 k^2\right] - I_\nu\right), \qquad (6)$$

where $\omega = \lambda/\gamma\mu_0 M_s$ is the dimensionless frequency,

$$(\omega_{\mathbf{k},\nu}^0)^2 = \left(\Delta \pm h_\nu - \Lambda^2 k^2\right)^2 - \Delta^2, \qquad (7)$$

is the dissipationless dispersion relation, and

$$\|\Psi_{\mathbf{k},\nu}\| = |u_{\mathbf{k},\nu}|^2 - |v_{\mathbf{k},\nu}|^2, \qquad (8)$$

is the norm of the two different branches of Eq. (3) [40]. In Fig. 1(b), we plot an example of the real part of the dispersion relation for both the left and right ferromagnets, with $h_L = 0.5$ and $h_R = 4.5$ and $\omega > 0$.

At this point, it is good to pause to emphasize a couple of things. First, the dissipationless limit of Eq. (3) is pseudo-Hermitian; in other words,

$$\sigma_z \mathcal{L}_\pm^\dagger \sigma_z = \mathcal{L}_\pm. \qquad (9)$$

A consequence of this is that the magnon norm $\|\Psi_{\mathbf{k},\nu}\|$ in Eq. (8) is conserved in the dissipationless limit. Second, Eq. (3) has the additional symmetry

$$\sigma_x(\mathcal{L}_\pm + i\alpha\omega^*\sigma_z + iI_\mu\mathbb{1})\sigma_x = -(\mathcal{L}_\pm - i\alpha\omega\sigma_z + iI_\mu\mathbb{1})^*. \qquad (10)$$

This implies that if ω is an eigenfrequency of Eq. (3) with eigenmode $(u_\nu \ v_\nu)^T$, then $-\omega^*$ is also an eigenfrequency with eigenmode $(v_\nu^* \ u_\nu^*)^T$. These two modes have opposite norms by construction. Hence, the two branches of Eq. (3) are related to each other via particle-hole symmetry. In our magnetic system, this doubling is not physical but is merely a result of our choice to describe spin waves using complex scalar fields. Hence, in order to describe the full dynamics of the system, it is sufficient to consider $\omega > 0$ and take into account the norms of different modes.

From this point onward, we refer to the positive-norm excitations as magnons and to the excitations carrying negative norm as antimagnons. This distinction between magnons and antimagnons is only allowed if we can solely consider excitation with a positive sign of ω, i.e., $\omega > 0$. Note that it is sufficient to consider $\omega > 0$, due to the particle doubling. We can make two important observations. First, antimagnons only exist in the right magnet. Second, antimagnons carry negative energy and, most importantly,

have opposite handedness with respect to the magnonic excitations.

The antimagnons in this setup can be stabilized, since in driven magnetic systems, energetic and dynamical stability do not necessarily coincide. For the system to be dynamically stable, we need

$$\mathrm{Im}(\omega_{\mathbf{k},\nu}) \simeq \mathrm{Im}\left(\omega_{\mathbf{k},\nu}^0\right) + \alpha\left[\Delta \pm h_\nu - \Lambda^2 k^2\right] - I_\nu > 0, \qquad (11)$$

for all wave numbers $\mathbf{k}$, because then small-amplitude fluctuations die out. This identity imposes that the magnons on the right side are dynamically stable if $-I_R \gtrsim \max\left[\alpha(h_R - \Delta), \Delta\right]$, whereas energetic instabilities exist if the (anti)magnon excitation energy is negative, i.e., $\|\Psi_{\mathbf{k},\nu}\| \omega_{\mathbf{k},\nu}^0 < 0$. We thus note that the magnons on the right FM are energetically unstable for a range of wave numbers but may be stabilized by injecting angular momentum via SOT (see Fig. 1). Physically, this means that the internal energy of the right ferromagnet can be lowered by small spin fluctuations (antimagnons) but injection of angular momentum prohibits the system from reaching a new ground state.

B. Exchange coupling at the interface

Additionally, the left and right thin films are exchange coupled [41], which results in effective boundary conditions for the magnetization. In terms of the Bogoliubov ansatz (5), the four boundary conditions follow from varying the energy functional in Eq. (2) after including the boundary term $E_{bn} = -J_c\mathbf{n}_L(0) \cdot \mathbf{n}_R(0)$ at the interface ($x = 0$). This gives

$$\Lambda\partial_x\varphi_L - \Lambda_c(\varphi_R + \varphi_L) = 0, \qquad (12a)$$

$$\Lambda\partial_x\varphi_R + \Lambda_c(\varphi_L + \varphi_R) = 0, \qquad (12b)$$

where $\varphi = u, v$ and $\Lambda_c = J_c/\Lambda\gamma\mu_0 M_s$. To analytically solve the scattering problem, we first focus on the isotropic case ($\Delta = 0$) and further show that the essential physics still holds for elliptical magnons ($\Delta \neq 0$).

III. SCATTERING OFF THE INTERFACE

Due to doubling of the modes, we consider $\omega > 0$ without loss of generality. Solutions of Eq. (3) without dissipative terms have the form

$$\begin{pmatrix} u(x) \\ v(x) \end{pmatrix} = \begin{pmatrix} u_k \\ v_k \end{pmatrix} e^{ikx}. \qquad (13)$$

At a given $\omega > \omega_{\min} \equiv h_L$, we find four different wave numbers k. In the left region with only positive-energy excitations, we find two real k_r^L, k_l^L and two complex k_+^L, k_-^L

wave numbers. These wave numbers are, according to Eq. (6), given by

$$\Lambda k_{r/l}^L = \pm\sqrt{\omega - h_L}, \quad \Lambda k_{\pm}^L = \pm i\sqrt{\omega + h_L}. \quad (14)$$

The complex modes are either blowing up or are damped, where only the damped mode is physically allowed [42]. However, in the right magnet—magnetized against the external magnetic field—there are four real wave numbers if $\omega < \omega_{max} \equiv h_R$, which are explicitly given by

$$\Lambda k_{r/l}^R = \pm\sqrt{\omega + h_R}, \quad \Lambda k_{\pm}^R = \pm\text{sgn}(\omega - h_R)\sqrt{h_R - \omega}. \quad (15)$$

The k_r and k_l modes correspond to positive-energy modes (magnons) with a positive and negative group velocity, respectively. Furthermore, k_+ and k_- correspond, respectively, to additional right- and left-moving modes carrying negative energy (antimagnons). We include $\text{sgn}(\omega - h_R)$ in the expression of $k_\pm$ here such that k_+ corresponds both to the right-moving negative-energy mode and the exponentially damped mode when $\omega > \omega_{max} \equiv h_R$.

We now construct the scattering solutions satisfying the boundary conditions in Eq. (12). The general solution for bulk modes at frequency ω are given by

$$u_\nu(x) = A_r^\nu u_{k_r,\nu} e^{ik_r x} + A_l^\nu u_{k_l,\nu} e^{ik_l x}$$
$$+ A_+^\nu u_{k_+,\nu} e^{ik_+ x} + A_-^\nu u_{k_-,\nu} e^{ik_- x}, \quad (16a)$$

$$v_\nu(x) = A_r^\nu v_{k_r,\nu} e^{ik_r x} + A_l^\nu v_{k_l,\nu} e^{ik_l x}$$
$$+ A_+^\nu v_{k_+,\nu} e^{ik_+ x} + A_-^\nu v_{k_-,\nu} e^{ik_- x}, \quad (16b)$$

where the A_j^ν are the amplitudes of the scattering modes in Eqs. (14) and (15) and the $(u_{k,\nu}, v_{k,\nu})$ are solutions to Eq. (3) with the ansatz given in Eq. (13) and the normalization condition $||u_{\nu,k}|^2 - |v_{\nu,k}|^2| = 1$. By disregarding spatially growing modes, the boundary conditions in Eq. (12) for magnons incident from the left imply

$$\mathbf{M} \begin{pmatrix} 1 \\ A_l^L \\ 0 \\ A_-^L \end{pmatrix} = \begin{pmatrix} A_v^R \\ 0 \\ A_+^R \\ 0 \end{pmatrix}. \quad (17)$$

Here, the matrix $\mathbf{M}$ is defined by the boundary conditions in Eq. (12) and is given by

$$\mathbf{M} = \frac{1}{\lambda_{u,l}^R - \lambda_{u,r}^R} \begin{pmatrix} 0 & 1 \\ 0 & 0 \end{pmatrix}$$

$$\otimes \begin{pmatrix} \lambda_{u,l}^R \lambda_{v,+}^L - 1 & \lambda_{u,l}^R \lambda_{v,-}^L - 1 \\ 1 - \lambda_{u,r}^R \lambda_{v,+}^L & 1 - \lambda_{u,r}^R \lambda_{v,-}^L \end{pmatrix}$$

$$+ \frac{1}{\lambda_{v,-}^R - \lambda_{v,+}^R} \begin{pmatrix} 0 & 0 \\ 1 & 0 \end{pmatrix}$$

$$\otimes \begin{pmatrix} \lambda_{v,-}^R \lambda_{u,r}^L - 1 & \lambda_{v,-}^R \lambda_{u,l}^L - 1 \\ 1 - \lambda_{v,+}^R \lambda_{u,r}^L & 1 - \lambda_{v,+}^R \lambda_{u,l}^L \end{pmatrix}, \quad (18)$$

where

$$\lambda_{\varphi,j}^L = +i\Lambda_c^{-1} \Lambda k_j - 1, \quad (19a)$$

$$\lambda_{\varphi,j}^R = -i\Lambda_c^{-1} \Lambda k_j - 1. \quad (19b)$$

By solving Eq. (17), we derive the reflection amplitudes as

$$A_l^L = -\frac{1 - \lambda_{v,+}^R \lambda_{u,r}^L}{1 - \lambda_{v,+}^R \lambda_{u,l}^L}, \quad A_-^L = 0. \quad (20)$$

We want to find the ratio between the incoming and reflected magnon spin currents. Here, we define the spin current as the spatial current following from the conservation of the norm—without dissipative terms—$\|\Psi\| = |u|^2 - |v|^2$, i.e., $-i\partial_t \|\Psi\| \mp \Lambda i\partial_x J_s = 0$. Using the equations of motion in Eq. (3), we find that the spin current is given by $iJ_s\Lambda = u\partial_x u^* - u^*\partial_x u + v\partial_x v^* - v^*\partial_x v$. Far from the interface, the Fourier transform of the spin current is dominated—for wave packets—by

$$J_s/\Lambda = \sum_{k_j} |A_j|^2 k_j \left(|u_{k_j}|^2 + |v_{k_j}|^2\right). \quad (21)$$

Finally, we derive the reflection coefficient as the ratio of the reflected and incident spin currents, by combining Eqs. (14), (20), and (21):

$$R^2 \equiv -J_s^R/J_s^I = |A_l^L|^2. \quad (22)$$

We now distinguish between the cases $\omega > h_R$ and $h_L < \omega < h_R$. (i) If $\omega > h_R$, then $|A_l^L|^2 = 1$; hence we have perfect reflection in this instance. (ii) If $h_L < \omega < h_R$, then the reflection coefficient becomes

$$R^2 = \frac{h_R - h_L + \Lambda_c^{-2}(\omega - h_L)(h_R - \omega) + 2\sqrt{\omega - h_L}\sqrt{h_R - \omega}}{h_R - h_L + \Lambda_c^{-2}(\omega - h_L)(h_R - \omega) - 2\sqrt{\omega - h_L}\sqrt{h_R - \omega}}. \quad (23)$$

For $\Lambda_c > \sqrt{h_R - h_L}/2$, the above expression is maximal at $\omega = (h_L + h_R)/2$, with the maximal reflection

$$R_{\text{max}}^2 = 1 + 8\Lambda_c^2/(h_R - h_L). \qquad (24)$$

On the other hand, if $\Lambda_c < \sqrt{h_R - h_L}/2$, the expression in Eq. (23) is maximal for $\omega = (h_R + h_L)/2 \pm \sqrt{(h_R + h_L)(h_R + h_L - 4\Lambda_c^2)/4}$ with the maximal reflection

$$R_{\text{max}}^2 = \frac{\sqrt{h_R - h_L} + |\Lambda_c|}{\sqrt{h_R - h_L} - |\Lambda_c|}. \qquad (25)$$

For both cases, we find the maximum reflection $R_{\text{max}} > 1$, which gives rise to spin-wave amplification and is the magnonic analog of the Klein paradox.

The physical picture of this anomalous reflection is illustrated in Fig. 1(c). Magnons with angular momentum (AM) $\hbar$ are excited in the left domain and incident at the interface. The overlap of the magnon band in the left magnet with the antimagnon band in the right magnet, produced by the unequal external fields, guarantees that the magnons can propagate into the right film. According to AM conservation, a magnon current with AM $\hbar$ propagating forward is expected to be produced in the right domain. However, magnons with AM $\hbar$ are forbidden due to the antiparallel orientation of the magnetization with respect to the external field. To conserve AM, antimagnon currents with AM $-\hbar$ propagating backward are generated and thus enlarge the reflected current. Throughout the scattering process, the group velocity of the transmitted antimagnons (v_g) is always positive, to guarantee the forward flow of energy. As a comparison, in the original Klein paradox, an electrostatic potential lifts the positron band in the right region and makes it overlap with the electron band in the incident region, while in the present case an inhomogeneous field lifts the antimagnon band and makes it overlap with the magnon band (see Appendix A).

IV. NUMERICAL VERIFICATION

To verify the analytical predictions and to account for effects of dissipation and nonlinearities, we perform micromagnetic simulations on two exchange-coupled ferromagnetic thin films as shown in Fig. 1(a) (for the simulation details, see Appendix B). Here, the interdomain coupling A_i is a tunable coefficient and is related to J_c in the theory as $J_c = -2A_i/d$. By applying a global driving microwave $\mathbf{h}(t) = h_0 \text{sinc}(\omega_c t)\hat{x}$ with $\omega_c/2\pi = 100$ GHz and $h_0 = 50$ mT, we first quantify the response of the magnetic system and identify two regimes as shown in Fig. 2. (i) When the current density $J > -1.4 \times 10^{12}$ A/m^2, the antiparallel state of the right domain ($\mathbf{n}_R \parallel -\mathbf{h}_R$) is dynamically unstable and the magnetization switches to the parallel state spontaneously ($\mathbf{n}_R \parallel \mathbf{h}_R$). The magnon spectrum of
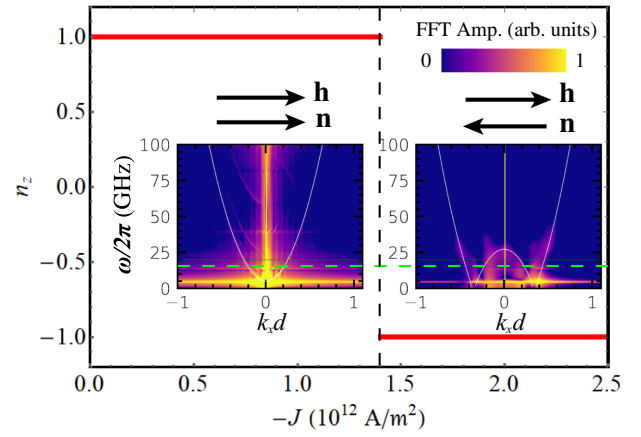

FIG. 2. The steady state n_z of the right magnet as a function of the current density (J) obtained by simulations. The inset shows the simulated magnon spectrum for $J = 0$ and -1.5×10^{-12} A/m^2, respectively. The white lines are the analytical dispersions. The horizontal dashed line is the driving frequency of the microwave ($\omega_0/2\pi = 20$ GHz) to initiate magnon scattering.

the right magnet for the steady parallel state is a normal parabola (left inset of Fig. 2) [43]. (ii) When $J < -1.4 \times 10^{12}$ A/m^2, the antiparallel state becomes dynamically stable, the antimagnon states in the negative-energy branch are excited, and a sombrerolike spectrum is identified (right inset of Fig. 2), consistent with the theory.

To study the magnon scattering off the interface between the left and right magnets, a microwave source $\mathbf{h}(t) = h_0 \sin(\omega_0 t)\hat{x}$ is applied at the left domain at $x = -d_{si}$, with $d_{si} = 800$ nm. The excited magnons propagate in the $+\hat{x}$ direction and scatter at the interface ($x = 0$). By making a Fourier transform of $n_x(x, y, t)$ in the propagating direction ($\hat{x}$) [45], we derive the response of the system in momentum space as shown in Fig. 3(a). An antimagnon state with $k_x < 0$ is clearly identified in the right domain while the reflection coefficient is larger than one. This demonstrates the enhancement of the magnon spin current via an analog of the Klein paradox. In the absence of injection, the antimagnon current is barely excited. A detailed analysis of the evolution of the incident, transmitted, and reflected magnon currents further verifies their correlation (see Appendix C).

Figure 3(b) shows that the reflected coefficient, defined as the peak height ratio of the reflection magnons and incident magnons, increases with the interdomain exchange coupling. For comparison, we also simulate the magnon scattering in the parallel configuration ($\mathbf{n}_R \parallel \mathbf{h}_R$) and find that the reflection keeps decreasing to zero with increasing coupling between the magnetic films (black diamonds). As expected, no antimagnon state is excited in this case. We find good agreement between the analytical prediction in Eq. (23) and the micromagnetic simulations for small couplings. For large exchange couplings, however, we see
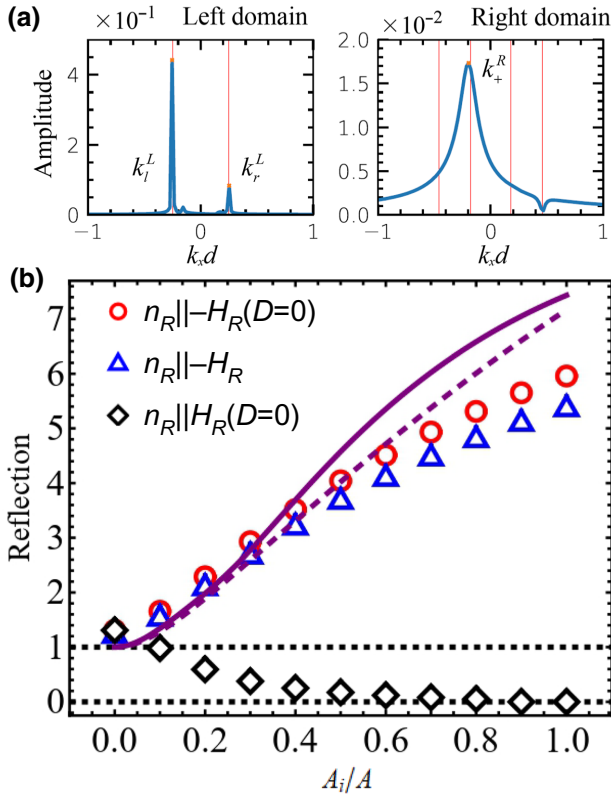
FIG. 3. (a) The scattering of magnons at the interface of left and right domains. $h_0 = 10$ mT, $A_i/A = 1$. The red vertical lines represent the theoretical predictions of the magnon wave vectors. (b) The reflection of magnons as a function of the interdomain exchange couplings. The Dzyaloshinskii-Moriya interaction (DMI) strength is $D = 0$ (red circles) and $D = 0.1$ mJ/m^2 [44] (blue triangles). The purple dashed line is predicted by Eq. (23) and the solid line is the prediction with shape anisotropy.

quantitative differences, which are not explained by the inclusion of dipolar anisotropy [see the purple solid line in Fig. 3(b)]. We expect the quantitative difference at large couplings to stem from nonlinear effects, which are not treated in the analytical formalism. The reflection amplitudes become increasingly large at increasing couplings, thereby making nonlinear effects important.

V. CONCLUSIONS

In conclusion, we show analytically and confirm numerically that the magnon spin current can be amplified through the realization of the bosonic Klein paradox in a driven-dissipative magnetic system. The Dzyaloshinskii-Moriya interaction (DMI) caused by the interfacial symmetry breaking in the hybrid system does not change the results significantly, as shown in Fig. 3(b). In our proposal, we dynamically stabilize the antimagnons by the SOT. The essential physics is applicable to a wide class of materials and driving "control knobs," which are able to maintain the magnetization against the external field; for example,

electric currents through spin-transfer torque [46], optical waves through magneto-optical interaction [47], and other effective techniques capable of producing a positive damping of the magnons. Our proposal can therefore be realized in ferromagnetic insulators as well as metals. Experimentally, the magnons may be detected by optical, inductive, and even electrical techniques [48–50].

APPENDIX A: DETAILED COMPARISON BETWEEN ORIGINAL AND MAGNON KLEIN PARADOX

In this appendix, we address the analog between the original Klein paradox and the magnon Klein paradox presented in the main text. In the original Klein paradox, Klein studied the scattering of an electron off a potential barrier [27], as shown in the top panel of Fig. 4(a). The electrostatic potential in the right domain will lift the negative energy band of positrons [blue line in Fig. 4(a)] and make it overlap with the positive energy band of electrons on the left (red line). Then, the incident electrons from the left domain can excite a positron current moving to the right in the right domain. This corresponds to a left-moving electron current and thus could enhance the reflection of electrons at the interface. A detailed treatment of this scattering process can be found in the literature [32]. In the magnon Klein paradox, an inhomogeneous external field, for example, can induce the band overlap of the magnon band in the left domain with the antimagnon band in the right domain, as shown in Fig. 4(b). Again, the antimagnon current generated at the interface enhances the strength of the reflected magnon current. The underlying physics of the original and the magnon Klein paradoxes is therefore the same. This is so despite the fact that the magnon bands on the left and right domains also overlap, but their coupling is very weak in our setup and thus this does not change the essential physics.
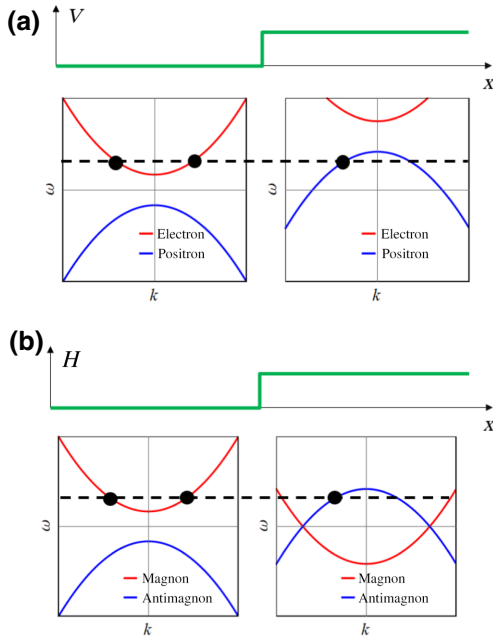
(a)

(b)

FIG. 4. A comparison between (a) the original and (b) the magnon Klein paradox. In each subfigure, the top panel (green line) sketches the "potential" distribution, while the bottom panel sketches the dispersion relation of particles (red lines) and antiparticles (blue lines).

APPENDIX B: PARAMETER SPECIFICATION IN NUMERICAL SIMULATIONS

The magnetization dynamics of the two exchange-coupled magnetic films are simulated by numerically solving Eq. (1). Note that the dissipation of the magnon spin current caused by its interaction with the environment is phenomenologically covered by the Gilbert damping, while identifying its microscopic mechanism, including spin-orbit interaction, spin pumping, and two-magnon scattering [13], is not the focus of our current work.

The dimensions of the nanostrip on each domain are length $l = 2048$ nm, width $w = 64$ nm, and thickness $d = 2$ nm. The SOT strength $J_L = 0$ and $J_R = J\hbar\theta_{SH}/(2M_s|e|d)$, where J is the current density, θ_{SH} is the spin-Hall angle of the heavy-metal layer, and e is the electron charge. Here, we use the magnetic parameters of YIG/Pt, i.e., the exchange coefficient $A = 3.1 \times 10^{-12}$ J/m, the saturation magnetization $M_s = 1.92 \times 10^5$ A/m, the spin-Hall angle $\theta_{SH} = 0.1$ [51], and the Gilbert damping $\alpha = 10^{-2}$. The interdomain coupling A_i is assumed to be a tunable coefficient and it is related to the coupling coefficient J_c in the theory as $J_c = -2A_i/d$. The mesh size is $2 \times 2 \times 2$ nm³. Absorptive boundary conditions are taken on the left domain to eliminate the influence of boundary reflection of magnons. The MUMAX³ [52] package is employed to numerically solve the LLG equation [Eq. (1)].

APPENDIX C: CORRELATIONS OF INCIDENT, REFLECTED, AND TRANSMITTED MAGNON SPIN CURRENT

In the main text, we consider a classical model in which the antimagnons in the right domain can only be excited by an incoming magnon current from the left domain dynamically stabilized by SOTs. Without an incoming spin current from the left magnet, the right domain stays in the dynamically stabilized state, where the magnetization is pointing against the external field. Continuous emission of antimagnons would be present in a quantum mechanical treatment of the problem, since there is no true ground state of the system. This can be interpreted as an analog of Hawking radiation. Since we are considering a classical theory in this paper, spontaneous emission of antimagnons is not captured by our classical model.

To verify the temporal correlation of antimagnon excitation and injected magnons, we plot the evolution of the
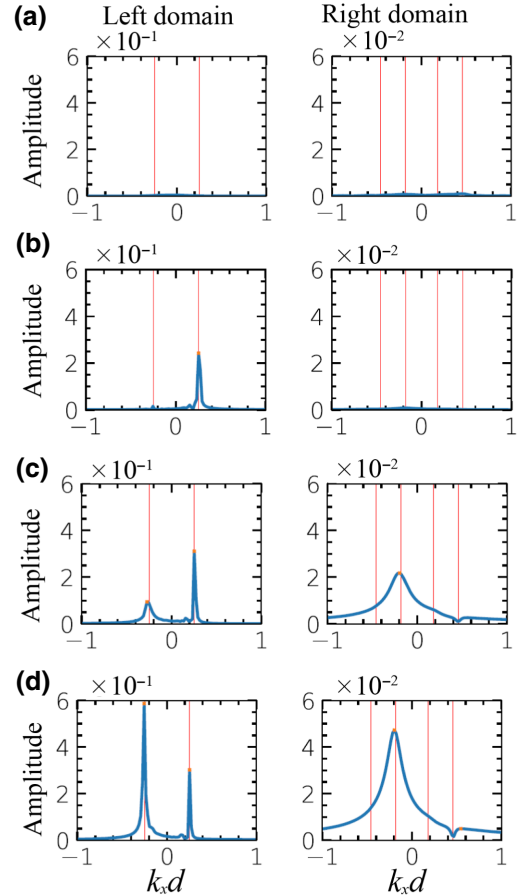

FIG. 5. The evolution of incident, reflected, and transmitted magnons at (a) $t = 0.05$ ns, (b) 0.5 ns, (c) 0.7 ns, and (d) 1.0 ns, respectively. The microwave source located in the left domain is turned on at $t = 0$ ns to excite magnons and then the magnons propagate toward the interface 800 nm away from the microwave source. All the other parameters are the same as in Fig. 3(a) of the main text.

incident, reflected, and transmitted magnon spin currents in Fig. 5. Right after the microwave source located in the left domain is turned on, the excitations of both magnons and antimagnons are nearly zero [Fig. 5(a)], where the tiny excitations mainly result from the fluctuation of spins in the ground state. Around 0.5 ns, the magnons in the left domain are significantly injected and propagate toward the interface [Fig. 5(b)]. At around 0.7 ns, the magnons reach the interface of the left and right domains and inject the antimagnon current into the right domain [Fig. 5(c)]. Meanwhile, the reflected spin current appears and is amplified. As more antimagnons are excited, the reflection also becomes stronger [Fig. 5(d)]. This indeed verifies the temporal correlation between the incident, reflected, and transmitted magnon spin currents.

[1] A. V. Chumak, V. I. Vasyuchka, A. A. Serga, and B. Hillebrands, Magnon spintronics, Nat. Phys. **11**, 453 (2015).

[2] M. Kostylev, A. Serga, T. Schneider, B. Leven, and B. Hillebrands, Spin-wave logical gates, Appl. Phys. Lett. **87**, 153501 (2005).

[3] K. Ganzhorn, S. Klingler, T. Wimmer, S. Geprägs, R. Gross, H. Huebl, and S. T. Goennenwein, Magnon-based logic in a multi-terminal YIG/Pt nanostructure, Appl. Phys. Lett. **109**, 022405 (2016).

[4] A. V. Chumak, A. A. Serga, and B. Hillebrands, Magnon transistor for all-magnon data processing, Nat. Commun. **5**, 1 (2014).

[5] H. Wu, L. Huang, C. Fang, B. Yang, C. Wan, G. Yu, J. Feng, H. Wei, and X. Han, Magnon Valve Effect between Two Magnetic Insulators, Phys. Rev. Lett. **120**, 097205 (2018).

[6] L. Cornelissen, J. Liu, B. Van Wees, and R. Duine, Spin-Current-Controlled Modulation of the Magnon Spin Conductance in a Three-Terminal Magnon Transistor, Phys. Rev. Lett. **120**, 097702 (2018).

[7] J. Cramer, F. Fuhrmann, U. Ritzmann, V. Gall, T. Niizeki, R. Ramos, Z. Qiu, D. Hou, T. Kikkawa, J. Sinova, U. Nowak, E. Saitoh, and M. Kläui, Magnon detection using a ferroic collinear multilayer spin valve, Nat. Commun. **9**, 1 (2018).

[8] J. Lan, W. Yu, R. Wu, and J. Xiao, Spin-Wave Diode, Phys. Rev. X **5**, 041049 (2015).

[9] H. Yuan, P. Yan, S. Zheng, Q. He, K. Xia, and M.-H. Yung, Steady Bell State Generation via Magnon-Photon Coupling, Phys. Rev. Lett. **124**, 053602 (2020).

[10] H. Yuan and R. A. Duine, Magnon antibunching in a nanomagnet, Phys. Rev. B **102**, 100402 (2020).

[11] H. Yuan, S. Zheng, Z. Ficek, Q. He, and M.-H. Yung, Enhancement of magnon-magnon entanglement inside a cavity, Phys. Rev. B **101**, 014419 (2020).

[12] D. Lachance-Quirion, S. P. Wolski, Y. Tabuchi, S. Kono, K. Usami, and Y. Nakamura, Entanglement-based single-shot detection of a single magnon with a superconducting qubit, Science **367**, 425 (2020).

[13] H. Yuan, Y. Cao, A. Kamra, R. A. Duine, and P. Yan, Quantum magnonics: When magnon spintronics meets quantum information science, Phys. Rep. **965**, 1 (2022).

[14] S. O. Demokritov, V. E. Demidov, O. Dzyapko, G. A. Melkov, A. A. Serga, B. Hillebrands, and A. N. Slavin, Bose-Einstein condensation of quasi-equilibrium magnons at room temperature under pumping, Nature **443**, 430 (2006).

[15] D. A. Bozhko, A. J. Kreil, H. Y. Musiienko-Shmarova, A. A. Serga, A. Pomyalov, V. S. L'vov, and B. Hillebrands, Bogoliubov waves and distant transport of magnon condensate at room temperature, Nat. Commun. **10**, 1 (2019).

[16] S. Takei and Y. Tserkovnyak, Superfluid Spin Transport through Easy-Plane Ferromagnetic Insulators, Phys. Rev. Lett. **112**, 227201 (2014).

[17] W. Yuan, Q. Zhu, T. Su, Y. Yao, W. Xing, Y. Chen, Y. Ma, X. Lin, J. Shi, R. Shindou, X. C. Xie, and W. Han, Experimental signatures of spin superfluid ground state in canted antiferromagnet Cr_2O_3 via nonlocal spin transport, Sci. Adv. **4**, eaat1098 (2018).

[18] O. Gladii, M. Collet, K. Garcia-Hernandez, C. Cheng, S. Xavier, P. Bortolotti, V. Cros, Y. Henry, J.-V. Kim, A. Anane, and M. Bailleul, Spin wave amplification using the spin Hall effect in permalloy/platinum bilayers, Appl. Phys. Lett. **108**, 202407 (2016).

[19] E. Padrón-Hernández, A. Azevedo, and S. Rezende, Amplification of Spin Waves by Thermal Spin-Transfer Torque, Phys. Rev. Lett. **107**, 197203 (2011).

[20] D. Malz, J. Knolle, and A. Nunnenkamp, Topological magnon amplification, Nat. Commun. **10**, 1 (2019).

[21] Y.-P. Wang, J. Rao, Y. Yang, P.-C. Xu, Y. Gui, B. Yao, J. You, and C.-M. Hu, Nonreciprocity and Unidirectional Invisibility in Cavity Magnonics, Phys. Rev. Lett. **123**, 127202 (2019).

[22] I. M. Miron, K. Garello, G. Gaudin, P.-J. Zermatten, M. V. Costache, S. Auffret, S. Bandiera, B. Rodmacq, A. Schuhl, and P. Gambardella, Perpendicular switching of a single ferromagnetic layer induced by in-plane current injection, Nature **476**, 189 (2011).

[23] L. Liu, O. Lee, T. Gudmundsen, D. Ralph, and R. Buhrman, Current-Induced Switching of Perpendicularly Magnetized Magnetic Layers Using Spin Torque from the Spin Hall Effect, Phys. Rev. Lett. **109**, 096602 (2012).

[24] K. Garello, I. M. Miron, C. O. Avci, F. Freimuth, Y. Mokrousov, S. Blügel, S. Auffret, O. Boulle, G. Gaudin, and P. Gambardella, Symmetry and magnitude of spin-orbit torques in ferromagnetic heterostructures, Nat. Nanotechnol. **8**, 587 (2013).

[25] A. Manchon, H. C. Koo, J. Nitta, S. Frolov, and R. Duine, New perspectives for Rashba spin-orbit coupling, Nat. Mater. **14**, 871 (2015).

[26] A. Manchon, J. Železný, I. M. Miron, T. Jungwirth, J. Sinova, A. Thiaville, K. Garello, and P. Gambardella, Current-induced spin-orbit torques in ferromagnetic and antiferromagnetic systems, Rev. Mod. Phys. **91**, 035004 (2019).

[27] O. Klein, Die Reflexion von Elektronen an einem Potentialsprung nach der relativistischen Dynamik von Dirac, Zeitschrift für Physik **53**, 157 (1929).

[28] N. Dombey and A. Calogeracos, Seventy years of the Klein paradox, Phys. Rep. **315**, 41 (1999).

[29] A. Hansen and F. Ravndal, Klein's paradox and its resolution, Phys. Scr. **23**, 1036 (1981).

[30] A. Nikishov, Barrier scattering in field theory removal of Klein paradox, Nucl. Phys. B **21**, 346 (1970).

[31] S. Gavrilov and D. Gitman, Quantization of charged fields in the presence of critical potential steps, Phys. Rev. D **93**, 045002 (2016).

[32] R. Brito, V. Cardoso, and P. Pani, *Superradiance* (Springer, 2020).

[33] J. D. Bjorken and S. D. Drell, *Relativistic Quantum Mechanics* (McGraw Hill College, New York, 1964).

[34] M. Katsnelson, K. Novoselov, and A. Geim, Chiral tunnelling and the Klein paradox in graphene, Nat. Phys. **2**, 620 (2006).

[35] N. Stander, B. Huard, and D. Goldhaber-Gordon, Evidence for Klein Tunneling in Graphene p-n Junctions, Phys. Rev. Lett. **102**, 026807 (2009).

[36] C. Gutiérrez, L. Brown, C.-J. Kim, J. Park, and A. N. Pasupathy, Klein tunnelling and electron trapping in nanometre-scale graphene quantum dots, Nat. Phys. **12**, 1069 (2016).

[37] C. Kittel, On the theory of ferromagnetic resonance absorption, Phys. Rev. **73**, 155 (1948).

[38] M. Sparks, Ferromagnetic resonance in thin films. III. Theory of mode intensities, Phys. Rev. B **1**, 3869 (1970).

[39] B. Kalinikos and A. Slavin, Theory of dipole-exchange spin wave spectrum for ferromagnetic films with mixed exchange boundary conditions, J. Phys. C: Solid State Phys. **19**, 7013 (1986).

[40] E. Lundh and H. M. Nilsen, Dynamic stability of a doubly quantized vortex in a three-dimensional condensate, Phys. Rev. A **74**, 063620 (2006).

[41] Here, the interface of the left and right domains may be a normal-metal layer that generates the interlayer exchange interaction between the left and right domains, an irradiated region where magnetic parameters can be effectively designed, or other regions that could induce an effective exchange coupling between the left and right domains.

[42] R. Verba, V. Tiberkevich, and A. Slavin, Spin-wave transmission through an internal boundary: Beyond the scalar approximation, Phys. Rev. B **101**, 144430 (2020).

[43] Here, the line shape of dispersion is consistent with the theoretical predictions (white lines), while we also note a series of standing-wave modes in the transverse direction ($k_y w = n\pi$, $n = 0, 1, 2, \ldots$). For a real magnetic film with a sufficiently larger width, the lower modes of the standing waves merge together. This does not have a significant influence on our results.

[44] H. Wang, J. Chen, T. Liu, J. Zhang, K. Baumgaertl, C. Guo, Y. Li, C. Liu, P. Che, S. Tu, S. Liu, P. Gao, X. Han, D. Yu, M. Wu, D. Grundler, and H. Yu, Chiral Spin-Wave Velocities Induced by All-Garnet Interfacial Dzyaloshinskii-Moriya Interaction in Ultrathin Yttrium Iron Garnet Films, Phys. Rev. Lett. **124**, 027203 (2020).

[45] Here, to eliminate the influence of magnons on the regions $x < -d_i$, which have the same wave vector and propagation direction as the reflecting magnons, the fast Fourier transform is only performed in the region between the microwave source and the interface, while a same-sized region is taken in the right domain.

[46] J. Wegrowe, M.-C. Ciornei, and H. Drouhin, Spin transfer in an open ferromagnetic layer: From negative damping to effective temperature, J. Phys.: Condens. Matter **19**, 165213 (2007).

[47] Y. Cao and P. Yan, Negative Gilbert damping, Phys. Rev. B **105**, 064418 (2022).

[48] T. Sebastian, K. Schultheiss, B. Obry, B. Hillebrands, and H. Schultheiss, Micro-focused Brillouin light scattering: Imaging spin waves at the nanoscale, Front. Phys. **3**, 35 (2015).

[49] V. Vlaminck and M. Bailleul, Spin-wave transduction at the submicrometer scale: Experiment and modeling, Phys. Rev. B **81**, 014425 (2010).

[50] L. Cornelissen, J. Liu, R. Duine, J. B. Youssef, and B. Van Wees, Long-distance transport of magnon spin information in a magnetic insulator at room temperature, Nat. Phys. **11**, 1022 (2015).

[51] H. Wang, C. Du, Y. Pu, R. Adur, P. C. Hammel, and F. Yang, Scaling of Spin Hall Angle in 3d, 4d, and 5d Metals from $Y_3Fe_5O_{12}$/Metal Spin Pumping, Phys. Rev. Lett. **112**, 197201 (2014).

[52] A. Vansteenkiste, J. Leliaert, M. Dvornik, M. Helsen, F. Garcia-Sanchez, and B. Van Waeyenberge, The design and verification of MuMax3, AIP Adv. **4**, 107133 (2014).